

Application of wavelets scaling function expansion method in resonance self-shielding calculation

Weiyang Yang*, Hongchun Wu, Youqi Zheng, Liangzhi Cao

School of Nuclear Science and Technology, Xi'an Jiaotong University, Xi'an Shaanxi 710049, China

ARTICLE INFO

Article history:

Received 16 October 2009

Received in revised form 25 January 2010

Accepted 11 February 2010

Available online 19 March 2010

Keywords:

Wavelets scaling function expansion

Resonance self-shielding calculation

Neutron

ABSTRACT

The wavelets expansion method is widely used in various fields due to its powerful ability to simulate the oscillating functions. This method is applied to discretize the energy variable of neutron angular flux within the resonant energy range. Meanwhile, the conventional multi-group method is applied in fast and thermal energy ranges. This coupled method can obtain the problem-dependent continuous-energy neutron flux spectrum within the resonant energy range. The method of characteristics (MOC) is employed as a space-variable solver in this paper to keep the powerful capability of dealing with the complex geometry problems. A pressurized water reactor (PWR) fuel cell problem with UO₂ fuel (UOX) and mixed oxide fuel (MOX), and a cylindrical cluster fuel problem are calculated by utilizing this coupled method. Results of these problems are all in good agreement with the results of the Monte Carlo statistical transport code MCNP. It is concluded that this is a valuable method to solve the resonance self-shielding calculation problems in a complex geometry, and it is promising to be applicable for realistic reactor problems.

© 2010 Elsevier Ltd. All rights reserved.

1. Introduction

Resonance self-shielding calculation is very important in reactor physics. In recent decades, many resonance self-shielding calculation methods have been developed, such as the Stamm'ler method and generalization of the Stamm'ler method (Hébert, 2007; Reuss and Coste-Delclaux, 2003). They are based on the equivalence theory between heterogeneous and homogeneous problems (Hébert and Marleau, 1991). The key process of these methods is calculating the fuel-to-fuel collision probability (CP). They are difficult to be extended to the complex geometry problems, although the generalization of the Stamm'ler method can solve complex geometry problems theoretically by the three-term rational approximation for CP. The Stamm'ler method has been used in lattice codes such as WIMS-AECL (Donnelly, 1986). The generalization of Stamm'ler method has been used in the code DRAGON (Marleau et al., 2000). For solving more complex geometry problems, the sub-group method (Nikolaev et al., 1970; Hébert, 2007; Reuss and Coste-Delclaux, 2003) discretizing the total cross-section instead of energy variable within the resonant energy range was developed. However, because the resonance parameters are processed under only single resonant nuclide

assumption, it has to calculate iteratively for multi-actinide problems. In recent years, although the sub-group method had been improved by increasing the sub-groups for this problem (Hébert, 2004; Coste-Delclaux, 2009), it is still a problem for resonance self-shielding calculation for MOX fuel, transmutation problems, etc., which contain multiple resonant nuclides. The number of sub-groups will be increased exponentially with the type of the resonant isotope. Therefore, the calculation efficiency will be reduced remarkably. This method has been utilized in the new versions of code CASMO (Knott et al., 1995), APOLLO2 (Sanchez et al., 1990) and HELIOS (Giust et al., 2001).

The advanced fuel design may be very complex and heterogeneous, and may contain various resonant nuclides, such as the application of MOX fuel and transmutation of minor actinides. The resonant nuclides will introduce very complicated resonance interference effects between these nuclides. Therefore hyper-fine energy group resonance calculation method (Tsuchihashi et al., 1983) and continuous-energy resonance calculation method (Williams and Asgari, 1995; Zhong et al., 2006) were developed. The hyper-fine energy group method divides the energy variable into tens of thousands of groups. The continuous-energy resonance calculation method applies a combination of multi-group and point-wise (PW) nuclear data. They all have the capability of obtaining the fine-structure energy distribution of the angular flux within the resonant energy range. However, the fine-structure neutron flux spectrum is obtained by interpolation of hyper-fine group fluxes or point-wise fluxes. Therefore, the spectrums obtained by

* Corresponding author. Address: No. 28 Xianning West Road, Xi'an 710049, PR China. Tel.: +86 029 82663285; fax: +86 029 82667802.

E-mail addresses: wyyang.xjtu@gmail.com (W. Yang), caolz@mail.xjtu.edu.cn (L. Cao).

these methods are not rigid continuous-energy flux spectrums. The hyper-fine energy group method and the continuous-energy resonance calculation method (PW resonance calculation method) have been implemented in the codes SRAC (Tsuchihashi et al., 1983) and SCALE5 (1990), respectively.

The theory of wavelets was developed by many researchers at the end of 1980s. It has several charming properties including localization property, local adaptability property and non-linear smoothing property, etc. Especially, the localization property makes it very powerful for simulating the function with severe oscillation. Because of these powerful properties, it has been well developed and widely applied in data compression, turbulence analysis, imaging and signal processing, etc. (Newland, 1993). In 1990s, it was applied to solve neutron diffusion equation by the wavelet Galerkin method (WGM) (Cho and Park, 1996). Recently, it was applied to solve the neutron transport problems in which the angular flux distributions along the azimuthal direction are fascinatingly complicated. Precise k_{eff} results and fine-structure angular distribution of the flux are obtained successfully (Buchan et al., 2008; Cao et al., 2008).

The neutron flux oscillates very violently within the resonant energy range because of the fierce oscillation of the total cross-section of resonant nuclides. According to this characteristic and the powerful properties of wavelets analysis, this paper introduces a new continuous-energy resonance calculation idea based on the wavelets scaling function expansion method. In this method, the energy variable of neutron angular flux is discretized by coupling the multi-group method and wavelets scaling function expansion method. Multi-group treatment is used within non-resonant energy ranges where the distributions of the fluxes are smooth. Concurrently, Daubechies' wavelets scaling function is employed to expand the energy variable of neutron angular flux within the resonant energy range.

More recently, Le Tellier et al. (2009) published their work with very similar idea with our work, even though we did our work independently. They expanded the resonant energy variable with wavelets function raised by Farras Abdelnour and Selesnick (2001). In our work, the wavelets scaling function, instead of the wavelets function, is employed to expand the energy variable of neutron angular flux. This difference will be explained in detail in the following section. Furthermore, in their work, only the homogeneous, single resonant nuclide problem is calculated under Livolant-Jeampierre hypotheses, the treatment of coupling relationship between the resonant energy range and non-resonant energy range is not considered. Besides, much effort of our work is dedicated to evaluating the accuracy of this method by numerical validation.

This paper is organized as follows. In Section 2, the fundamental properties of the wavelets scaling function and the theoretical model of the method are described. In Section 3, four testing problems are calculated and discussed. Finally, Section 4 provides the conclusions of this work.

2. Theoretical model

2.1. Basics of wavelets theory

The functions named 'wavelets' are translated and dilated from a single function (Cho and Park, 1996). They are defined by a dilation and translation operation as:

$$\psi_{n,k}(x) = 2^{n/2} \psi(2^n x - k), \quad \psi \in L^2(\mathbb{R}), \quad n, k \in \mathbb{Z} \quad (1)$$

The scaling function is the generator of wavelet function. It has the same form as:

$$\varphi_{n,k}(x) = 2^{n/2} \varphi(2^n x - k), \quad \varphi \in L^2(\mathbb{R}), \quad n, k \in \mathbb{Z} \quad (2)$$

here n is the 'dilation order'. \mathbb{Z} and \mathbb{R} denote the set of integers and real numbers, respectively.

$L^2(\mathbb{R})$ denotes the space of measurable, square – integrable functions.

Suppose we define

$$\mathbf{V}_n = \text{span}\langle \varphi_{n,k} : k \in \mathbb{Z} \rangle \quad (3)$$

and

$$\mathbf{W}_n = \text{span}\langle \psi_{n,k} : k \in \mathbb{Z} \rangle \quad (4)$$

Then the scaling functions and the wavelet functions have the following sub-space relations:

$$\dots \mathbf{V}_{-1} \subset \mathbf{V}_0 \subset \mathbf{V}_1 \subset \mathbf{V}_2 \dots \quad (5)$$

$$\mathbf{V}_n = \mathbf{V}_{n-1} \oplus \mathbf{W}_{n-1} \quad (6)$$

$$\bigcup_n \mathbf{V}_n = L^2(\mathbb{R})$$

and

$$\bigoplus_n \mathbf{W}_n = L^2(\mathbb{R}) \quad (7)$$

where \oplus stands for orthogonal summation.

From Eq. (6), we can obtain

$$\mathbf{V}_n = \mathbf{V}_{n-m} \oplus \mathbf{W}_{n-m} \oplus \dots \oplus \mathbf{W}_{n-2} \oplus \mathbf{W}_{n-1} \quad (8)$$

Based on Eqs. (6) and (7), wavelets decomposition at scale n becomes:

$$\begin{aligned} \mathbf{f}_n(\mathbf{x}) &= \sum_k \mathbf{a}_{n,k} \varphi_{n,k}(\mathbf{x}) \\ &= \sum_k \mathbf{a}_{n-m,k} \varphi_{n-m,k}(\mathbf{x}) + \sum_{j=n-m}^{n-1} \sum_k \mathbf{b}_{n-m,k} \psi_{j,n}(\mathbf{x}) \end{aligned} \quad (9)$$

In Eq. (9), the expression expands function \mathbf{f} at a single scale n , while the second expression expands a multi-scale representation of \mathbf{f} at the scales $\{n-m, \dots, n-2, n-1\}$.

From Eqs. (5) and (7), sufficiently large values of n exist such that $\|\mathbf{f} - \mathbf{f}_n\|$ is arbitrarily small for any $\mathbf{f} \in L^2$.

If we define that $\varphi \in \mathbf{V}_0$ and $\psi \in \mathbf{W}_0$, there are the following two-scale relations from Eq. (6):

$$\varphi(x) = \sum_k \mathbf{c}_k \varphi(2x - k)$$

and

$$\psi(x) = \sum_k \mathbf{d}_k \psi(2x - k). \quad (10)$$

The two-scale relations are applied for construction of the scaling and wavelets functions. If ψ is required to generate orthonormal basis, the coefficients \mathbf{c}_k and \mathbf{d}_k have the following relation:

$$\mathbf{d}_k = (-1)^k \mathbf{c}_{1-k} \quad (11)$$

In this paper, we apply the Daubechies' wavelets, which are constructed by Daubechies (2001). They are defined as a kind of orthonormal and compactly supported wavelets in the following form:

$$\varphi_{n,k}(x) = \sum_{j=2k}^{2N+2k-1} c_{j-2k} \varphi_{n+1,j}(x) \quad (12)$$

and

$$\psi_{n,k}(x) = \sum_{j=2k-2N+2}^{2k-1} (-1)^j c_{1-j+2k} \varphi_{n+1,j}(x) \quad (13)$$

where c represents the Daubechies' coefficients and N is the Daubechies' order, n is the dilation order, k and l are translation subscripts.

They have many special and powerful properties (Cho and Park, 1996; Daubechies, 2001):

$$\begin{aligned} \text{support}(\varphi_{n,k}) &= [2 - nk, 2 - n(k + 2N - 1)] \\ \text{and support}(\psi_{n,k}) &= [2 - n(k + 1 - N), 2 - n(k + N)] \\ \varphi_{n,k}, \psi_{n,k} &\in C^{\lambda(N)} \\ &= \text{the space of Holder continuous functions with exponent } \lambda(N). \end{aligned} \quad (14)$$

$$\int \psi_{n,k}(\mathbf{x}) \mathbf{x}^m d\mathbf{x} = 0 \text{ for all integer } n, \text{ and any integer } 0 \leq m < N - 1. \quad (16)$$

$$\|\mathbf{f} - \mathbf{f}_n\| < C \|\mathbf{f}\| 2^{-Nn}. \quad (17)$$

$$\int \varphi_{n,k}(x) dx = 1. \quad (18)$$

$$\int \varphi_{n,k}(x) \varphi_{n,l}(x) dx = \delta_{k,l},$$

$$\text{and } \int \psi_{n,k}(x) \psi_{n,l}(x) dx = \delta_{n,m} \delta_{k,l}. \quad (19)$$

Here $\delta_{k,l}$ is the Delta function.

Eq. (14) shows that the width of the support region of the wavelets and scaling function is related to the Daubechies' order N and the dilation order n . The larger the Daubechies' order N is, the wider of the supporting region of scaling function will be. It also can be seen from Eq. (15) that the larger N is, the smoother the scaling function will be. Fig. 1 gives examples of the scaling function whose Daubechies' orders are $N=3$ (Fig. 1a) and $N=5$ (Fig. 1b), respectively (dilation order n and k is set to be zero). Eq. (17) comes from Strang's work (1989), which states that smooth functions can be approximated with error $O(h^N)$ by combinations at every scale $h = 2^{-n}$.

Eq. (18) denotes the weighing property of individual Daubechies' scaling function in the decomposition. Eq. (19) represents the orthonormal property, which is important in obtaining the expansion moment equations in the decomposition. The weighing and orthonormal properties can reduce the computing work when we integrate the product of the scaling functions and the wavelets functions. Daubechies (2001) pointed out other properties of the Daubechies' scaling function. The method of construction of Daubechies' wavelets scaling function was shown in the paper of Cho and Park in detail.

2.2. Fundamental idea of wavelets scaling function expansion method

The fundamental idea of the method is to discretize the energy variable of neutron angular flux by coupling the multi-group method and wavelets scaling function expansion method, which is

shown in Fig. 2. The conventional multi-group method is utilized in the non-resonant energy ranges. The resonant energy range is divided into several resonant groups first. This division is the same as the conventional multi-group method. The angular flux is expanded with wavelets scaling function in each resonant energy group.

The energy variable of the angular flux is discretized by wavelets scaling functions within each resonant group as:

$$\Phi(\vec{r}, \mathbf{E}, \vec{\Omega}) = \sum_l \mathbf{a}_{il}(\vec{r}, \vec{\Omega}) \varphi_{il}(\mathbf{E}) \quad l = 1, 2, \dots, \mathbf{p} \quad (20)$$

Here i is the dilation order, N the Daubechies' order, l translation subscript, $\mathbf{a}_{il}(\vec{r}, \vec{\Omega})$ is the wavelets scaling function expansion moments. $\mathbf{p} = 2^i + 2N - 2$ is the total number of wavelets scaling functions applied in single resonant group.

Then, we can obtain the fine-structure of neutron spectrum using Eq. (11) if the expansion moments $\mathbf{a}_{n,k}(\vec{r}, \vec{\Omega})$ are obtained. The steady-state neutron transport equation is represented as:

$$\begin{aligned} \vec{\Omega} \cdot \nabla \Phi(\vec{r}, E, \vec{\Omega}) + \Sigma_t(\vec{r}, E) \Phi(\vec{r}, E, \vec{\Omega}) \\ = \int_0^\infty \int_0^{4\pi} \Sigma_s(\vec{r}, E' \rightarrow E, \vec{\Omega}' \rightarrow \vec{\Omega}) \Phi(\vec{r}, E', \vec{\Omega}') d\vec{\Omega}' dE' \\ + \frac{\chi(E)}{4\pi k} \int_0^\infty \int_0^{4\pi} \nu(E') \Sigma_f(\vec{r}, E') \Phi(\vec{r}, E', \vec{\Omega}') d\vec{\Omega}' dE' \end{aligned} \quad (21)$$

here $\vec{\Omega}$ is the neutron flight direction, \vec{r} is the space coordinate, E is the energy, $\Sigma_t(\vec{r}, E)$ is the macroscopic total cross-section, $\Sigma_s(\vec{r}, E' \rightarrow E, \vec{\Omega}' \rightarrow \vec{\Omega})$ is the double-differential scatter cross-section, $\chi(E)$ is the fission spectrum, $\nu(E)$ is the number of neutron per fission, $\Sigma_f(\vec{r}, E)$ is the macroscopic fission cross-section.

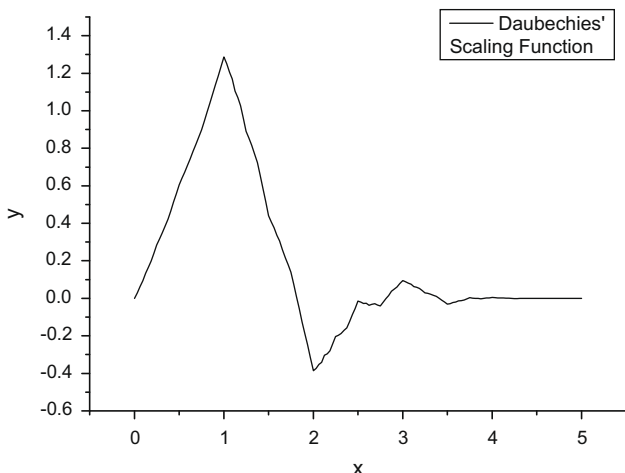
Substituting Eq. (11) into Eq. (12), a set of equations about the expansion moments by utilizing the orthogonality of Daubechies' wavelets scaling function is obtained. Fortunately, the form of expansion moment equations is similar with the neutron transport equation. It is written as:

$$\vec{\Omega} \cdot \nabla \mathbf{a}_{il}(\vec{r}, \vec{\Omega}) + \sum_n \mathbf{a}_{in}(\vec{r}, \vec{\Omega}) \mathbf{A}_{l,n} = \mathbf{S}_l + \mathbf{F}_l \quad l = 1, 2, \dots, \mathbf{p} \quad (22)$$

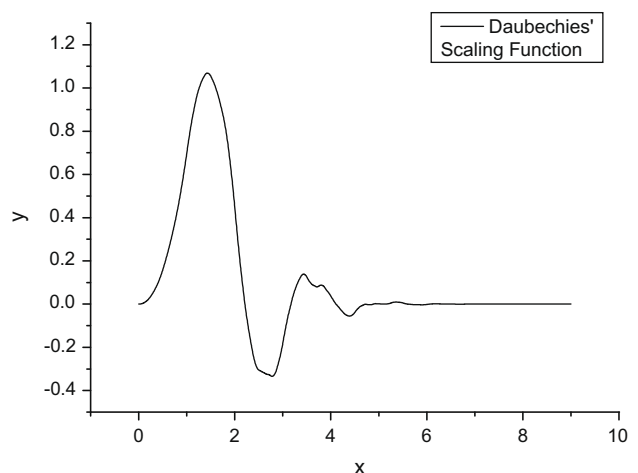
or $\mathbf{B} \times \mathbf{a} = \mathbf{Y}$.

Here, $\mathbf{B}_{l,n} = \delta_{l,n} (\vec{\Omega} \cdot \nabla) + \sum_n \mathbf{A}_{l,n}$ is the element of the matrix, $\mathbf{a} = (\mathbf{a}_{i,1}, \mathbf{a}_{i,2}, \dots, \mathbf{a}_{i,p-1}, \mathbf{a}_{i,p})^T$ is the expansion coefficient matrix, $\mathbf{Y} = (\mathbf{S}_1 + \mathbf{F}_1, \mathbf{S}_2 + \mathbf{F}_2, \dots, \mathbf{S}_{p-1} + \mathbf{F}_{p-1}, \mathbf{S}_p + \mathbf{F}_p)^T$ is the matrix of the sources.

$$\text{Define a matrix } \mathbf{A} = (\mathbf{A}_{l,n}) \quad l \in [0, \mathbf{p}], n \in [0, \mathbf{p}] \quad (23)$$



(a) Daubechies' order $N=3$



(b) Daubechies' order $N=5$

Fig. 1. Distribution of Daubechies' scaling function.

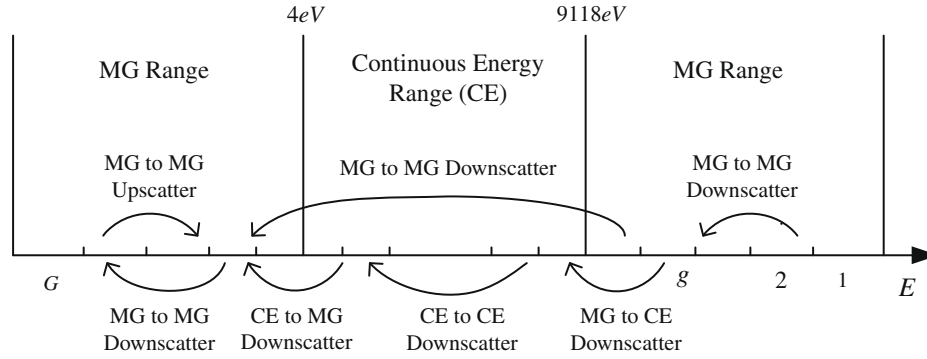


Fig. 2. Scheme of the coupling method of wavelets scaling function expansion and multi-group treatment.

The parameters of the equations $A_{l,n}$, S_l and F_l are represented as:

$$A_{l,n} = \int_{\Delta E_g} \Sigma_t(\vec{r}, E) \varphi_{i,l}(E) \varphi_{i,n}(E) dE = A_{n,l}, \quad (24)$$

$$S_l = \int_{\Delta E_g} \varphi_{i,l}(E) \int_0^\infty \int_0^{4\pi} \Sigma_S(\vec{r}, E' \rightarrow E, \vec{\Omega}' \rightarrow \vec{\Omega}) \Phi(\vec{r}, E', \vec{\Omega}') d\vec{\Omega}' dE' dE, \quad (25)$$

and

$$F_l = \frac{1}{4\pi k} \int_{\Delta E_g} \varphi_{i,l}(E) \chi(E) \int_0^\infty \int_0^{4\pi} v(E') \Sigma_f(\vec{r}, E') \Phi(\vec{r}, E', \vec{\Omega}') d\vec{\Omega}' dE' dE. \quad (26)$$

Moving the non-diagonal elements of the Eq. (22) to the right side of the equation, the equation is changed to

$$\vec{\Omega} \cdot \nabla \mathbf{a}_{i,l}(\vec{r}, \vec{\Omega}) + \mathbf{a}_{i,l}(\vec{r}, \vec{\Omega}) \mathbf{A}_{l,l} = \mathbf{S}_l + \mathbf{F}_l - \sum_{n \neq l} \mathbf{a}_{i,n}(\vec{r}, \vec{\Omega}) \mathbf{A}_{l,n} \quad (27)$$

Thus, it can be calculated in the following iterative scheme:

$$\vec{\Omega} \cdot \nabla \mathbf{a}_{i,l}^j(\vec{r}, \vec{\Omega}) + \mathbf{a}_{i,l}^j(\vec{r}, \vec{\Omega}) \mathbf{A}_{l,l} = \mathbf{S}_l^{j-1} + \mathbf{F}_l^{j-1} - \sum_{n \neq l} \mathbf{a}_{i,n}^{j-1}(\vec{r}, \vec{\Omega}) \mathbf{A}_{l,n} \quad (28)$$

Here j is the iteration superscript.

After showing the method of the wavelets scaling function expansion, we will describe the differences of this method and Le Tellier's scheme. In this method, the first expression of Eq. (9) is utilized. The expansion is done in sub-space \mathbf{V}_i . We know from Eq. (24) that the parameter matrix \mathbf{A} is symmetric. Also, the matrix \mathbf{A} is a band matrix because the Daubechies' wavelets scaling function is a compactly supported function. The width of the matrix is $4N - 3$, which is determined by the Daubechies' order N . Usually, the matrix is dominant diagonal. Therefore, the expansion coefficient equations shown in Eq. (22) are loosely coupled. The simple iterative scheme shown in Eq. (28) is available, and the iterative calculation of expansion coefficient equations will not noticeably increase the calculation cost. While in the work of Le Tellier et al., the second expression of Eq. (9) is applied, the expansion is done in sub-space $\mathbf{V}_0 + \sum_{j=0}^J \mathbf{W}_j$. The expansion basis is combined with $\varphi_{0,k}(\mathbf{x})$ and $\psi_{j,k}(\mathbf{x})$, which makes the expansion coefficient equations tightly coupled. Therefore, a modification method is applied to decouple the equations. In the work of Zheng et al. (2009), they also applied wavelets scaling function instead of wavelets function for the expansion basis to make the tightly coupled expansion coefficient equations sparsely coupled. Numerical

results validate that it is good for improving the calculation efficiency in the work of Zheng et al.

All of parameters $A_{l,n}$, S_l and F_l can be calculated with the multi-group and continuous-energy nuclear cross-section data. They are therefore constants when we calculate Eq. (27). Because the form of Eq. (27) is similar with standard multi-group neutron transport equation, the existing methods to solve the neutron transport equation can be utilized directly. In this paper, the method of characteristics (MOC) (Askew, 1972; Chen et al., 2008) is applied to solve the neutron transport and the expansion moment equations. The MOC is capable of solving the complex geometry neutron transport problems, because it solves the neutron transport equation along the characteristic lines. Therefore, the wavelets scaling function expansion method introduced by this paper is capable of solving the complex geometry problems. The expansion moment equations are derived from the steady-state neutron transport equation, so the continuous-energy neutron flux within the resonant energy range and the infinite multiplication factor (k -inf) can be obtained directly. Meanwhile, the multi-group neutron cross-sections within resonant energy range are processed by utilizing the continuous-energy neutron flux as the weighing function. It is shown as:

$$\Sigma_g = \frac{\int_{\Delta E_g} \Sigma(\mathbf{E}) \Phi(\mathbf{E}) d\mathbf{E}}{\int_{\Delta E_g} \Phi(\mathbf{E}) d\mathbf{E}} = \frac{\sum_k \mathbf{a}_{n,k} \int_{\Delta E_g} \varphi_{n,k}(\mathbf{E}) \Sigma(\mathbf{E}) d\mathbf{E}}{\sum_k \mathbf{a}_{n,k} \int_{\Delta E_g} \varphi_{n,k}(\mathbf{E}) d\mathbf{E}} \quad (29)$$

As we know, the WIMS data library (Halsall, 1991) gives out the values of effective resonant integral for several dilution cross-sections and different temperatures, and the results of effective resonant integral are processed under the single resonant nuclide assumption. In this case, the iterative calculation has to be utilized for the multi-actinide resonant problems in conventional self-shielding calculation method by assuming that other resonant nuclides are non-resonant. However, in the wavelets scaling function method the iterative calculation is unnecessary for multi-actinide resonant problems because the continuous-energy nuclear cross-section data and s-wave elastic scattering law are applied within the resonant range.

From Eq. (22), we know that if we know the parameters $A_{l,n}$, S_l and F_l , we can calculate the equation iteratively applying the iterative scheme shown in Eq. (28). The parameter $A_{l,n}$ can be computed numerically. While for S_l and F_l , they have to be represented with wavelets scaling expansion coefficients firstly. Therefore, in the following two sections we will describe the treatment of them in detail.

2.3. Scattering source calculation

The angular-dependence of the differential macroscopic scattering cross-section is represented by a finite Legendre expansion of order L :

$$\Sigma(E' \rightarrow E; \mu_0) = \sum_{l=0}^L \frac{2l+1}{2} \Sigma_l(E' \rightarrow E) P_l(\mu_0) \quad (30)$$

where L is the order of the Legendre expansion, μ_0 cosine of scatter angle, measured in the laboratory coordinate system, $P_l(\mu_0)$ the Legendre polynomials evaluated at the laboratory scattering cosine, and $\Sigma_l(E' \rightarrow E)$ is the cross-section moment which is defined by the expression:

$$\Sigma_l(E' \rightarrow E) = \int_{-1}^1 \Sigma(E' \rightarrow E; \mu_0) P_l(\mu_0) d\mu_0 \quad (31)$$

Substituting the Legendre expansion for the scattering cross-section and using spherical harmonic addition theorem (O'Dell and Alcouffe, 1987), the scattering source is represented as:

$$\begin{aligned} \mathbf{S}(\vec{r}, \mathbf{E}, \vec{\Omega}) &= \int_0^\infty \int_0^{4\pi} \Sigma(\vec{r}, \mathbf{E}' \rightarrow \mathbf{E}, \vec{\Omega}' \rightarrow \vec{\Omega}) \Phi(\vec{r}, \mathbf{E}', \vec{\Omega}') d\vec{\Omega}' dE' \\ &= \sum_{lk=0}^{LK} \frac{2l+1}{2} \mathbf{Y}_{lk}(\vec{\Omega}) S_{lk}(\vec{r}, E) \end{aligned} \quad (32)$$

where $Y_{lk}(\vec{\Omega})$ are the spherical harmonic functions, and $S_{lk}(\vec{r}, E)$ are spherical harmonic moments of the scattering source. They are written as:

$$\begin{aligned} S_{lk}(E) &= \int_{E'} S_{lk}(E' \rightarrow E) dE' \\ &= \int_{E'} \Sigma_l(E' \rightarrow E) \Phi_{lk}(E') dE' \end{aligned} \quad (33)$$

where $\Phi_{lk}(E)$ are the spherical harmonic moments of the angular flux, which are defined as:

$$\Phi_{lk}(E) = \int_0^{4\pi} Y_{lk}(\vec{\Omega}) \Phi(\vec{\Omega}) d\vec{\Omega} \quad (34)$$

The parameters $S_{lk}(E' \rightarrow E)$ are the moments of the differential scattering rate from energy $E' \rightarrow E$, which are represented as:

$$S_{lk}(E' \rightarrow E) = \Sigma_l(E' \rightarrow E) \Phi_{lk}(E') \quad (35)$$

Within the non-resonant energy range, calculation of the scatter source is the same as multi-group method which is unnecessary to be iterated. However, within the resonant energy range, there are two cases needed to be treated specifically. For the first case the neutrons are scattered from fast neutron energy range, the other case's neutrons are scattered from resonant energy range itself.

Similar to the WIMS data library, we suppose the resonant energy range is from 4 eV to 9118 eV. If the energy $< 10/A^{2/3}$ MeV (A is the atomic mass number), the scattering will be elastic scattering. Therefore, the scattering within resonant energy range is elastic scattering, and the s-wave elastic scattering law (Bell and Glasstone, 1970) can be applied for most of the nuclides. It is represented as:

$$f(\vec{r}, E' \rightarrow E; \vec{\Omega}' \rightarrow \vec{\Omega}) = \begin{cases} \frac{1}{(1-\alpha)E'} \delta(\vec{\Omega}' \cdot \vec{\Omega} - \mu_0), \alpha E' < E < E' \\ 0, E < \alpha E'; E > E' \end{cases} \quad (36)$$

where $\alpha = \left(\frac{A-1}{A+1}\right)^2$ and $\mu_0 = \frac{1}{2}[(A+1)\sqrt{E/E'} - (A-1)\sqrt{E'/E}]$. $\delta(x)$ denotes the Dirac-delta function.

For the first case where neutrons are scattered from the fast neutron energy range, an energy-dependent intra-group distribution function $y(E)$ is introduced to the spherical harmonic moments of the scatter source. Then the moments of spherical harmonic function expansion of scattering source are written as (Williams and Asgari, 1995; Zhong et al., 2006):

$$S_{lk}(E) = S_{lk,g} \frac{y_l(E)}{\int_{\Delta E_g} y_l(E) dE} \quad (37)$$

Inserting the s-wave elastic scattering kernel in Eq. (36) into the cross-section moments in Eq. (31), the cross-section moments become

$$\Sigma_l(E' \rightarrow E) = \frac{\Sigma(E')}{(1-\alpha)E'} P_l(G(E', E)) \quad (38)$$

Then the spherical harmonic function expansion moments of scattering source are represented as:

$$\begin{aligned} S_{lk}(E) &= \int_{E'} S_{lk}(E' \rightarrow E) dE' = \int_{E'} \Sigma_l(E' \rightarrow E) \Phi_{lk}(E') dE' \\ &= \int_{E'} \frac{\Sigma(E')}{(1-\alpha)E'} P_l(G(E', E)) \Phi_{lk}(E') dE' \end{aligned} \quad (39)$$

From Eqs. (37) and (39), the P_0 and P_1 distribution functions of elastic scattering source from hydrogen can be rigorously expressed as:

$$y_0(E) = c, c > 0 \quad (40a)$$

$$y_1(E) = E \quad (40b)$$

The higher moments of the hydrogen scatter source can be neglected, because they are less important than the first two moments. For other nuclides, only the first order shown as Eq. (40a) is applied in Williams and Asgari's paper because obtaining the higher order moments is very complicated, also the moments with higher orders are less important. Finally the scattering source from fast neutron energy region to resonant energy region from nuclide j is represented as:

$$\begin{aligned} S_{j,g,he}^j &= \int_{\Delta E_g} \phi_{i,l}(\mathbf{E}) \int_0^\infty \int_0^{4\pi} \Sigma_S^j(\vec{r}, \mathbf{E}' \rightarrow \mathbf{E}, \vec{\Omega}' \rightarrow \vec{\Omega}) \Phi(\vec{r}, \mathbf{E}', \vec{\Omega}') d\vec{\Omega}' dE' d\mathbf{E} \\ &= \int_{\Delta E_g} \phi_{i,l}(\mathbf{E}) \sum_{lk} \frac{2l+1}{2} \mathbf{Y}_{lk}(\vec{\Omega}) S_{lk}^j(\vec{r}, \mathbf{E}) d\mathbf{E} \\ &= \begin{cases} \sum_{lk} \frac{2l+1}{2} \mathbf{Y}_{lk}(\vec{\Omega}) S_{lk,g}^j \frac{\int_{\Delta E_g} \phi_{i,l}(\mathbf{E}) y_l(\mathbf{E}) d\mathbf{E}}{\int_{\Delta E_g} y_l(\mathbf{E}) d\mathbf{E}}, & j \in H_1 \\ \sum_{lk} \frac{2l+1}{2} \mathbf{Y}_{lk}(\vec{\Omega}) S_{lk,g}^j \frac{\int_{\Delta E_g} \phi_{i,l}(\mathbf{E}) d\mathbf{E}}{\Delta E_g}, & j \neq H_1 \end{cases} \end{aligned} \quad (41)$$

here ΔE_g is energy region of the g th group, 'he' means the neutrons of scattering source are scattered from the fast neutron energy range.

Substituting Eqs. (32) and (39) into Eq. (25), the scattering source from the g' th group to the g th group is obtained.

$$\begin{aligned} S_{n,g' \rightarrow g} &= \int_{\Delta E_g} \phi_{i,n}(E) \sum_{lk=0}^{LK} \frac{2l+1}{2} Y_{lk}(\vec{\Omega}') S_{lk}(E) dE \\ &= \sum_{lk=0}^{LK} \frac{2l+1}{2} Y_{lk}(\vec{\Omega}') \int_{\Delta E_g} \phi_{i,n}(E) \int_{\Delta E_{g'}} \frac{\Sigma(E')}{(1-\alpha)E'} P_l(G(E', E)) \Phi_{lk}(E') dE' dE \end{aligned} \quad (42)$$

here the g' th group and the g th group are all resonant groups.

Substituting the wavelets scaling function expansion of the flux represented as Eq. (20) into Eq. (42) and taking $l=0$ as an example, the P_0 scattering source scattering from the g' th group to the g th group is represented as:

$$\begin{aligned} S_{n,g' \rightarrow g} &= \int_{\Delta E_g} \phi_{i,n}(E) \int_{\Delta E_{g'}} \int_0^{4\pi} \Sigma_0(\vec{r}, \mathbf{E}' \rightarrow \mathbf{E}, \vec{\Omega}' \rightarrow \vec{\Omega}) \times \Phi(\vec{r}, \mathbf{E}', \vec{\Omega}') d\vec{\Omega}' dE' dE \\ &= \frac{1}{(1-\alpha)} \int_{\Delta E_g} \phi_{i,n}(E) dE \sum_m \int_{\Delta E_{g'}} \frac{\Sigma_S(E') \phi_{i,m}(E')}{E'} dE' \int_{4\pi} a_{i,m}(\vec{r}, \vec{\Omega}') d\vec{\Omega}' \end{aligned} \quad (43)$$

The scattering source represented with wavelets scaling function expansion coefficients is finally obtained. Thus the scattering source can be computed with the coefficients.

2.4. Fission source calculation

In multi-group method the fission source (O'Dell and Alcouffe, 1987) can be expressed as:

$$F_g = \frac{\chi_g}{4\pi k} \sum_{g'} v \Sigma_{f,g'}(\vec{r}) \Phi_{g'}(\vec{r}) \quad (44)$$

Using the wavelets scaling function expansion of flux within resonant energy range, the total production of neutron in resonant group g' is written as:

$$\begin{aligned} S_{f,g'}(\vec{r}) &= \int_{\Delta E_{g'}} \int_0^{4\pi} v(E') \Sigma_f(\vec{r}, E') \Phi(\vec{r}, \vec{\Omega}', E') dE' d\vec{\Omega}' \\ &= \sum_n \int_0^{4\pi} a_{i,n}(\vec{r}, \vec{\Omega}') d\vec{\Omega}' \int_{\Delta E_{g'}} v(E') \Sigma_f(\vec{r}, E') \varphi_{i,n}(E') dE' \end{aligned} \quad (45)$$

Then the fission source within the non-resonant energy range can be written as:

$$F_g = \frac{\chi_g}{4\pi k} \left[\sum_{g' \neq RA} v \Sigma_{f,g'}(\vec{r}) \Phi_{g'}(\vec{r}) + \sum_{g' \in RA} S_{f,g'}(\vec{r}) \right] \quad (46)$$

where 'RA' means the resonant energy range.

Similarly, the fission sources within resonant energy range are given as:

$$\begin{aligned} F_{l,g} &= \int_{\Delta E_g} \varphi_{i,l}(E) \frac{\chi(E)}{4\pi k} \int_0^{4\pi} v(E') \Sigma_f(\vec{r}, E') \Phi(\vec{r}, \vec{\Omega}', E') d\vec{\Omega}' dE' \\ &= \frac{1}{4\pi k} \left[\int_{\Delta E_g} \varphi_{i,l}(E) \chi(E) dE \right] \left[\sum_{g' \neq RA} v \Sigma_{f,g'}(\vec{r}) \Phi_{g'}(\vec{r}) + \sum_{g' \in RA} S_{f,g'}(\vec{r}) \right] \end{aligned} \quad (47)$$

Thus, the fission source can be computed with the wavelets scaling function expansion coefficients and the group fluxes of non-resonant groups as shown in Eq. (47).

The Maxwell fission spectrum or the Watt fission spectrum is used in the resonant energy range, which is shown in Table 1 in detail. Briesmeister (2000) gives out fission spectrum constants of other fissionable isotopes which are not presented in Table 1. Meanwhile, the fission spectrum from the WIMS nuclear data library is utilized within the non-resonant energy range.

The Maxwell fission spectrum and the Watt fission spectrum (Briesmeister, 2000) can be represented as following, respectively:

$$f(E) = C \cdot E^{1/2} \cdot \exp(-E/a) \quad (48)$$

$$f(E) = C \cdot \exp(-E/a) \cdot \sinh(bE)^{1/2} \quad (49)$$

here C is the normalization constant.

3. Numerical results

A special MOC code is chosen as the angular and spatial variable solver of multi-group neutron transport and wavelets scaling function expansion coefficient equations in this work. In this MOC code, AutoCAD is customized to carry out the ray tracing procedure with a high flexibility in geometry. The description of complex geometry becomes quite efficient and convenient because of the powerful graphics capability of AutoCAD. The ray tracing procedure can be implemented uniformly regardless of the geometry shape by using the language Visual Basic for Applications (VBAs) to customize AutoCAD. Therefore, this MOC code has powerful capability of solving complex geometry problems. In the paper of Chen et al., the implementation and numerical validation of this kind of MOC are described in detail.

In this paper, the multi-group nuclear data come from the WIMS 69-group library based on jeff31 issued by IAEA. The resonant groups are from the 15th group to the 27th group. The energy division of groups in the resonant range is the same as multi-group library. The continuous-energy nuclear data come from the MCNP4C continuous-energy nuclear data library named endf602. We know that the reason of the neutron flux oscillating very violently within the resonant energy range is the fierce oscillation of the total cross-section of resonant nuclides in that energy range. According to the MCNP4C continuous-energy nuclear data, the resonant groups with higher energy are close to the unresolved resonant energy range, which contain more resonance peaks with smaller heights compared to lower energy resonant groups. Therefore, for different resonant groups, the orders of wavelets scaling function expansion should be different. From Eq. (17), the larger the dilation order n and the Daubechies' order N are, the better results will be obtained. However, from Eq. (22), increasing n and N will also increase the amount of the expansion coefficient equations, which will increase the calculation cost. Thus, it is an important problem for selecting appropriate orders for different resonant groups to obtain the balance between precision and calculation efficiency.

3.1. Selecting orders of wavelets scaling expansion

The fierce oscillations of the neutron spectrum are due to the peaks of the total cross-section of resonant nuclides. Therefore, we can estimate the expansion orders of different resonant group by applying wavelets scaling function expansion for simulating the total cross-section. The total cross-section of resonant nuclide is expanded with wavelets scaling function like this:

Table 1
Parameters of fission spectrums utilized for different fissionable isotopes.

The Maxwell fission spectrum			The Watt fission spectrum			
Fissionable isotope	E_{in} (MeV) ^a	a (MeV)	Fissionable isotope	E_{in} (MeV)	a (MeV)	b (MeV ⁻¹)
$n + {}^{238}\text{Pu}$	Thermal	1.330	$n + {}^{232}\text{Th}$	Thermal	1.0888	1.6871
	1	1.330		1	1.1096	1.6316
	14	1.330		14	1.1700	1.4610
$n + {}^{240}\text{Pu}$	Thermal	1.346	$n + {}^{235}\text{U}$	Thermal	0.988	2.249
	1	1.3615		1	0.988	2.249
	14	1.547		14	1.028	2.084
$n + {}^{241}\text{Pu}$	Thermal	1.3597	$n + {}^{238}\text{U}$	Thermal	0.88111	3.4005
	1	1.3752		1	0.89506	3.2953
	14	1.5323		14	1.96534	2.8330
$n + {}^{242}\text{Pu}$	Thermal	1.337	$n + {}^{239}\text{Pu}$	Thermal	0.966	2.842
	1	1.354		1	0.966	2.842
	14	1.552		14	1.055	2.383

^a E_{in} is the incident neutron energy.

$$\Sigma_t(\mathbf{E}) = \sum_l \mathbf{a}_{n,l} \varphi_{n,l}(\mathbf{E}) \quad l = 1, 2, \dots, 2^n + 2N - 2 \quad (50)$$

and $\mathbf{a}_{n,l} = \int_{\Delta E} \Sigma_t(\mathbf{E}) \varphi_{n,l}(\mathbf{E}) d\mathbf{E} \quad l = 1, 2, \dots, 2^n + 2N - 2$

Integrating the continuous-energy total cross-section, the integrated total cross-section is obtained:

$$\Sigma_{t,g} = \sum_l \mathbf{a}_{n,l} \int_{\Delta E_g} \varphi_{n,l}(\mathbf{E}) d\mathbf{E} \quad l = 1, 2, \dots, 2^n + 2N - 2 \quad (51)$$

here $\Sigma_{t,g}$ is the integrated total cross-section of the g th group.

We take the 27th group total cross-section of uranium-238 for an example. Fig. 3 shows the continuous-energy total cross-section of uranium-238 from the continuous-energy data library of MCNP4C. It is seen that most part of the cross-section is smooth, though there is a big peak standing about from 6.5 eV to 7.0 eV. In the paper of Cho and Park it is suggested that for smooth function the Daubechies' order $N \geq 4$ is good enough that the scaling function can be chosen as the expansion basis. Therefore, the Daubechies' order N is set to be 5 in this paper. Fig. 4 shows the behavior of the simulating as N changed from 3 to 5. Fig. 5 shows the behavior of the simulating as the dilation order changed from 5 to 7. We can see that the results of the cross-section simulation become better as the dilation order increases. The simulation obtains a good result when the dilation order n reach 7. If the dilation order is not large enough such as $n = 5$, the peak will be broadened as shown in the Fig. 5. The errors of the group total cross-section are shown in Fig. 6. The errors reduce along with n and N increasing. Although $n = 7$ is good enough for the 27th group, the dilation orders have to be set larger for the higher energy resonant groups, because the total cross-sections are more complicated in those resonant groups. We set two cases of dilation orders for different resonant groups to analyze the convergence of this method along with increasing the dilation order. The cases of dilation orders are shown in Table 2.

A computation code named WAVRESON has been implemented based on the model introduced above. Three problems are calculated to validate this method. The first problem is a PWR pin-cell problem. The results are calculated under 10 conditions with different enrichments. The second problem is the MOX fuel problem with the same geometry as the PWR pin-cell problem. The third problem is a cylindrical cluster geometry problem. It is calculated to validate the capability of solving

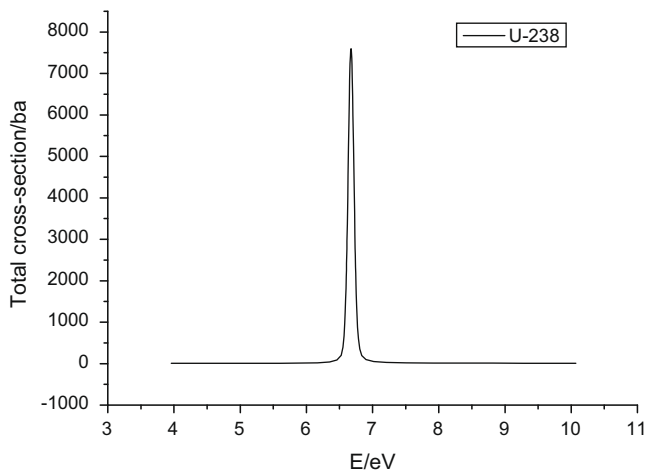


Fig. 3. The 27th group total cross-section of uranium-238.

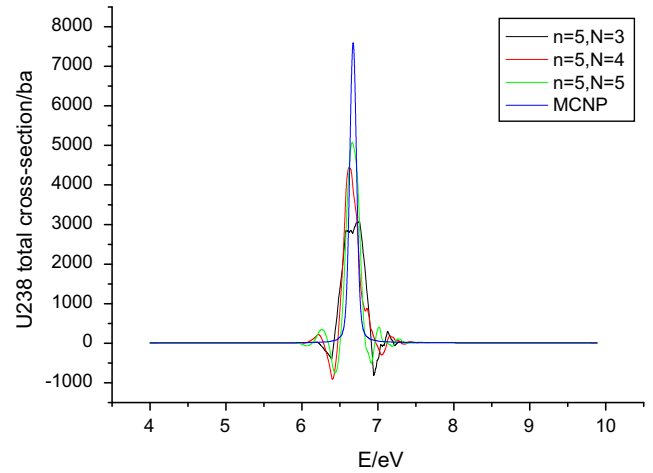


Fig. 4. Simulation of the 27th group uranium-238 total cross-section.

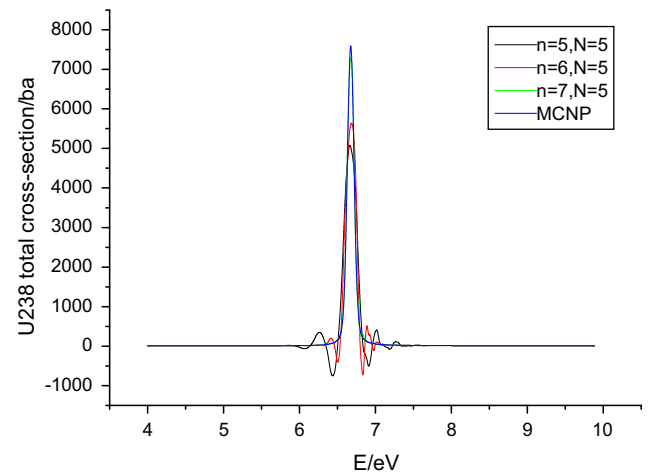


Fig. 5. Simulation of the 27th group uranium-238 total cross-section.

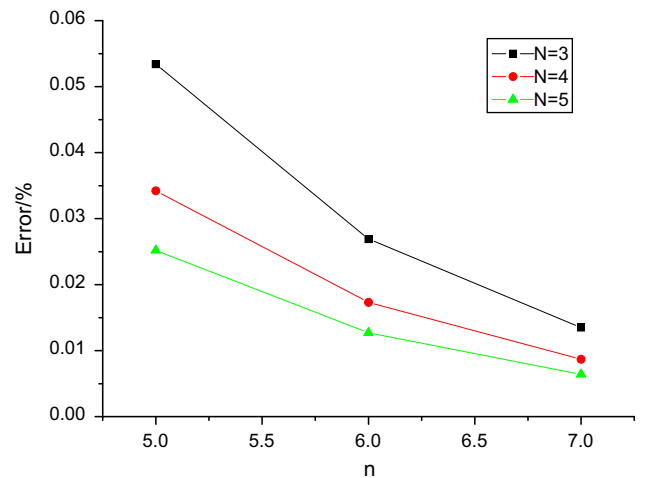


Fig. 6. The simulation errors of uranium-238 integrated total cross-section of the 27th group.

complex geometry problems. They are shown in the following paragraphs.

Table 2
Dilation orders for different resonant groups.

Group	15th	16th	17th	18th	19th	20th	21st	22nd	23rd	24th	25th	26th	27th
Case 1	8	8	8	8	8	8	8	8	7	7	7	7	7
Case 2	9	9	9	9	9	9	9	8	8	7	7	7	7

3.2. PWR fuel cell problem

The first problem is a PWR fuel cell problem shown in Fig. 7. The cell is subdivided into seven regions, and the track spacing is 0.01 cm. Regions 1 and 2 are water, region 3 is cladding, and the regions from 4 to 7 are fuel. The size of the PWR fuel cell is 1.26 cm × 1.26 cm, the radii of the cladding and fuel are 0.475 cm and 0.4095 cm, respectively. The material compositions are shown in Table 3, and different nuclide densities are shown in Table 4.

In MCNP calculation, 20,000 particles are put for each generation and 250 generations are tallied, 50 of which are disregarded. From the results in Table 5, it is seen that the results of Case 2 are better than those of Case 1, which means that increasing the dilation orders is effective for improving the accuracy. All of the results are smaller than those calculated by MCNP except the 3%, 5%, and 7% enrichment situations in Case 2. The reason for this phenomenon is that in this method the resonant peaks of flux within the resonant energy range will be broadened, if the dilation orders of the wavelet scaling function expansion are not large enough. The phenomena also can be seen in Fig. 5. The broadened flux of resonant energy range will increase the resonant absorption and make the k -inf smaller than the reference value. It is similar to the phenomena of Doppler broadening, which also makes the k -inf smaller than reference value. It also indicates the reason why increasing the dilation orders can improve the results. The improvements of the results for lower enrichment cases are more remarkable than the higher enrichment cases, because the resonant effects of ^{238}U within high energy resonant groups are much more severe than those of ^{235}U . The errors of uranium-238 total cross-section reaction rate compared with MCNP are presented in Table 6. It is seen that increasing the dilation orders is also beneficial to improve the accuracy of the total cross-section reaction rate of uranium-238.

Fig. 8 is the fine-structure flux spectrum of the 4th region in 15% enrichment condition, which shows that the fine-structure neutron spectrum in the fuel of three-zone PWR fuel cell problem agrees with the result of MCNP well. The reason for the differences on the left side of the lines is disregarding the neutron up-scattering

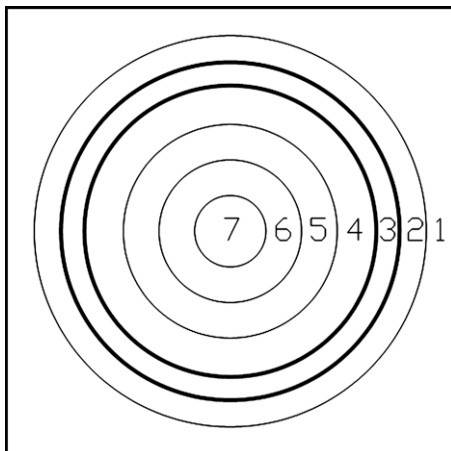


Fig. 7. Geometry of the PWR fuel cell.

Table 3
Material composition of the PWR fuel cell.

Material	Atomic density (10^{24} atom/cm 3)			
	$^{235}\text{U} + ^{238}\text{U}$	^{16}O	^1H	Zr-nature
Fuel	0.0230934	0.0461868	–	–
Cladding	–	–	–	0.04360
Water	–	0.03362	0.06723	–

Table 4
Densities of nuclides within fuel region of different enrichments.

Enrichment (%)	Atomic density (10^{24} atom/cm 3)		
	^{235}U	^{238}U	^{16}O
3	0.00070140	0.02239200	0.0461868
5	0.00115467	0.02193873	0.0461868
7	0.00161654	0.02147686	0.0461868
10	0.00230934	0.02078406	0.0461868
15	0.00346401	0.01962939	0.0461868
30	0.00692802	0.01616538	0.0461868
50	0.01154670	0.01154670	0.0461868
70	0.01616538	0.00692802	0.0461868
90	0.02078406	0.00230934	0.0461868
100	0.02309340	0.0	0.0461868

from the thermal energy range. From Table 6, although there are some differences in the left side of the continuous-energy fluxes, the bias of the 27th group total reaction rate of uranium-238 is less than 1.0%. Therefore, the bias introduced by disregarding the up-scattering from the thermal energy range to the resonant energy range is small. Actually, for multi-group neutron transport calculation, the up-scattering from the thermal energy range to the resonant energy range is always not taken into consideration.

To compare the calculation accuracy with the standard resonance self-shielding calculation method, we calculate the same PWR pin-cell problem with DRAGON, which applies the generalization of Stamm'ler method as the resonance self-shielding calculation method. The 69 multi-group library based on nuclear data file jeff31 is used. The results are presented in Fig. 9. We can see that WEVERESON is more accurate compared with DRAGON, especially in the high enrichment cases.

Another problem is the MOX fuel problem (Worrall, 1999). The geometry of this problem is same as PWR cell problem. The fuel is changed to the MOX fuel. The atomic densities of the MOX fuel are in Table 7. The compositions of cladding and water are same as the PWR cell problem. In the MCNP calculation, 10,000 particles are put for each generation and 250 generations are tallied, 20 of which are disregarded. From Table 7, we can see that there are seven kinds of resonant nuclides in MOX fuel. Therefore, the resonance interference effects between the resonant nuclides are noticeable. The results are shown in Table 8, increasing the dilation order is also beneficial for improving the accuracy. The enrichment of plutonium is significant for the accuracy of MOX problem because of the resonant interference effect. We can predict that the larger weight ratio is and the more kinds of resonant nuclides there are, the larger dilation orders are needed, because resonant interference effects are more severe and the flux spectrums are more complicated within resonant energy range.

Table 5
The k-inf results of PWR fuel cell.

Enrichment (%)	MCNP k-inf	Case 1 ^a		Case 2 ^b	
		WAVERESON k-inf	Error (%)	WAVERESON k-inf	Error (%)
3	1.38497 ± 0.00035	1.383085	-0.135	1.387733	0.199
5	1.48563 ± 0.00023	1.482164	-0.233	1.487005	0.093
7	1.53626 ± 0.00027	1.531529	-0.308	1.536376	0.008
10	1.57835 ± 0.00030	1.572394	-0.377	1.577137	-0.077
15	1.61687 ± 0.00031	1.609771	-0.439	1.614251	-0.162
30	1.67677 ± 0.00029	1.669067	-0.459	1.672689	-0.243
50	1.73173 ± 0.00027	1.724503	-0.417	1.727086	-0.268
70	1.77958 ± 0.00027	1.773553	-0.339	1.775217	-0.245
90	1.82811 ± 0.00025	1.822348	-0.315	1.823204	-0.268
100	1.86524 ± 0.00025	1.859690	-0.298	1.860425	-0.258

^a The Case 1 dilation orders shown in Table 2 are utilized.
^b The Case 2 dilation orders shown in Table 2 are utilized.

Table 6
The errors of uranium-238 total cross-section reaction rate compared with MCNP.

Group	Error/%	
	Case 1	Case 2
15th	4.574	1.943
16th	4.977	2.091
17th	6.529	1.567
18th	4.563	0.664
19th	3.201	0.371
20th	4.797	1.002
21st	1.924	0.555
22nd	0.265	0.344
23rd	-0.321	-0.465
24th	0.784	0.853
25th	0.390	0.453
26th	-0.543	-0.482
27th	-0.888	-0.828

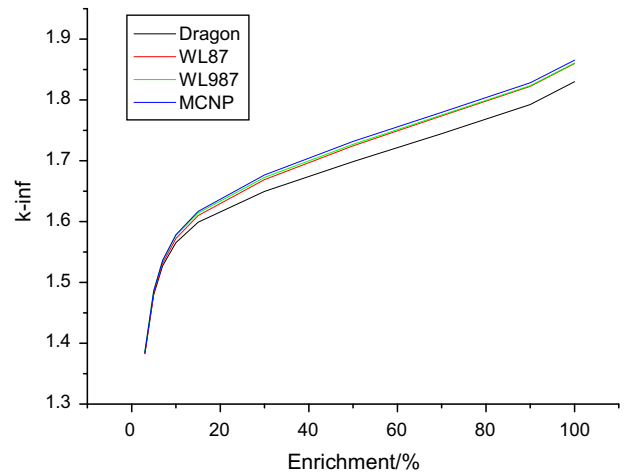


Fig. 9. Comparison the results of WAVERESON and DRAGON with MCNP.

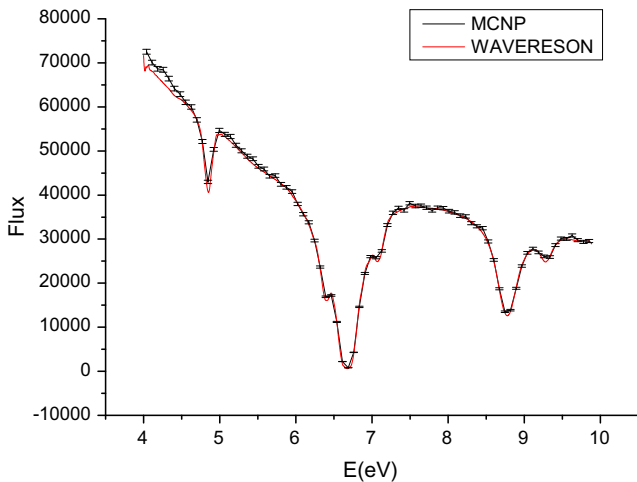


Fig. 8. Fine-structure neutron spectrum of the resonant group (the 27th group).

3.3. Cylindrical cluster geometry problem

Marleau et al. (2000) gave out the cylindrical cluster geometry problem. The geometry of this problem is shown in Fig. 10. The material components and atomic densities of the fuel region are the same as 3% enrichment case of the PWR cell problem shown in Table 4. Beyond the fuel region is light water, the atomic densities of oxygen and hydrogen are the same as PWR cell case shown in Table 3. In MCNP calculation, 10,000 particles are put for each generation and 250 generations are tallied, 20 of which

Table 7
Densities of the MOX fuel.

Nuclide	Atomic density (10 ²⁴ atom/cm ³)	
	Case I	Case II
¹⁶ O	4.683197E-02 ^a	4.682251E-02
²³⁵ U	1.127624E-03	1.091347E-03
²³⁸ U	2.115426E-02	2.047369E-02
²³⁸ Pu	2.809131E-05	4.573003E-05
²³⁹ Pu	6.219000E-04	1.012395E-03
²⁴⁰ Pu	2.962335E-04	4.822405E-04
²⁴¹ Pu	1.072423E-04	1.745804E-04
²⁴² Pu	8.063234E-05	1.312619E-04

^a Read as 4.683197 × 10⁻².

are disregarded. A good result is obtained shown in Table 9, although the problem has complicated geometry and unstructured distribution fuel.

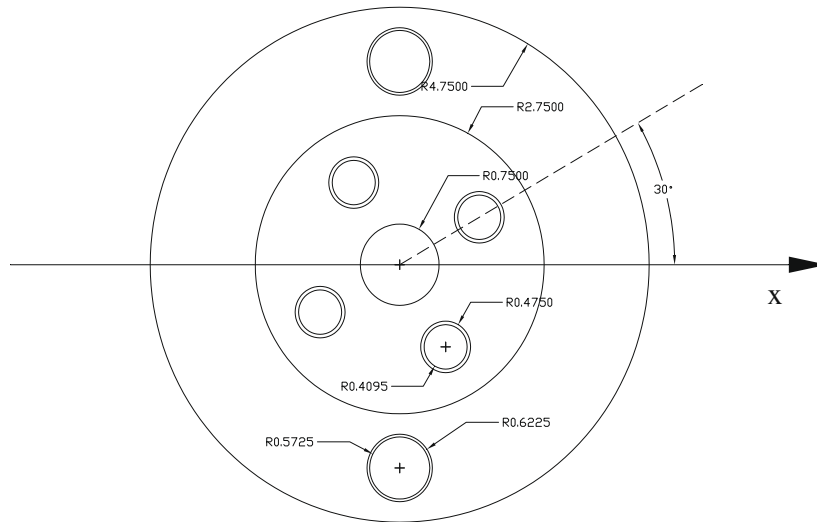
4. Conclusion

This paper presents an innovative method for resonance self-shielding calculations. In this method, the energy variable of the neutron angular flux in resonant energy range is dealt with by utilizing wavelets scaling function expansion method. Some preliminary numerical results demonstrate that the wavelet scaling function expansion method is capable of calculating k-inf and problem-dependent fine-structure neutron spectrum within

Table 8

The k-inf results of the MOX fuel problem.

PU enrichment (%)	MCNP k-inf	Case 1 ^a		Case 2 ^b	
		WAVRESON k-inf	Error (%)	WAVRESON k-inf	Error (%)
Case I	1.32382 ± 0.00046	1.319134	−0.354	1.323242	−0.058
Case II	1.31622 ± 0.00044	1.305828	−0.790	1.309789	−0.489

^a The Case 1 dilation orders shown in Table 2 are utilized.^b The Case 2 dilation orders shown in Table 2 are utilized.**Fig. 10.** Geometry of cylindrical cluster geometry problem.**Table 9**

The k-inf results of cylindrical cluster geometry problem.

MCNP	WAVRESON ^a	Error (%)
0.83149 ± 0.00033	0.829768	−0.207

^a The Case 1 dilation orders shown in Table 2 are utilized.

resonant energy range with good accuracy. Moreover, this method has other advantages compared to conventional resonance methods. First, this method is capable of solving complicated geometry resonant calculation problems, if the transport calculation method which has the ability to solve complex geometry problems is applied. Secondly, there is no more iterative calculation needed in this method even the fuel consists of more than one resonant nuclide. Thirdly, the rigid continuous-energy flux spectrum rather than the pseudo continuous-energy flux spectrum calculated by interpolating point-wise fluxes in the PW continuous-energy resonance method is obtained, because the Daubechies' wavelets scaling function utilized as the expansion basic function of the flux is a continuous function. Fourthly, this method is more efficient than PW resonant calculation method. In this method, the neutron transport equation is transformed to a set of expansion moment equations within the resonant energy range. Even applying the Case 2 dilation orders shown in Table 2, there are totally less than 4900 equations, which are much less than those of the PW method. However, continuous-energy data coming from MCNP nuclear data library are applied within the resonant energy range while the multi-group data coming from WIMSD4 format nuclear data library are used in the non-resonant energy range. The data file compatibility is therefore another issue which should be concerned in further calculation. This can be improved by processing the continuous-energy data and multi-group data by NJOY (Farlane and Boicourt, 1975) correspondingly to maintain the coherence.

Acknowledgments

This work is supported by National Natural Science Foundation of China Grants No. 10875094, No. 10605017, and by the National High Technology Research and Development Program ("863" program) of China No. 2009AA050705.

References

- Askew, R., 1972. A Characteristics Formulation of the Neutron Transport Equation in Complicated Geometries, AEEW-M, 1108.
- Bell, G.L., Glasstone, S., 1970. Nuclear Reactor Theory. Van Nostrand, Princeton, New Jersey.
- Briesmeister, J.F., 2000. MCNP-A General Monte Carlo N-Particle Transport Code. LA-13709M.
- Buchan, A.G., Pain, C.C., Eaton, M.D., Smedley-Stevenson, R.P., Goddard, A.J.H., 2008. Self-adaptive spherical wavelets for angular discretizations of the Boltzmann transport equation. Nucl. Sci. Eng. 158, 244–263.
- Cao, L., Wu, H., Zheng, Y., 2008. Solution of neutron transport equation using Daubechies' wavelets expansion in the angular discretization. Nucl. Eng. Des. 238, 2292.
- Chen, Q., Wu, H., Cao, L., 2008. Auto MOC-A 2D neutron transport code for arbitrary geometry based on the method of characteristics and customization of AutoCAD. Nucl. Eng. Des. 238, 2828.
- Cho, N.Z., Park, C.J., 1996. Wavelets theory for solution of the neutron diffusion equation. Nucl. Sci. Eng. 124, 417.
- Coste-Delclaux, M., 2009. Recent progress in self-shielding phenomenon modeling with the APOLL02 code. Trans. Am. Nucl. Soc. 100, 652–653.
- Donnelly, J.V., 1986. WIMS-CRNL, A User's Manual for the Chalk River Version of WIMS. AECL-8955, Atomic Energy of Canada Limited.
- Daubechies, I., 2001. Ten Lecture on Wavelets. Rutgers University and AT&T Bell Lab.
- Farlane, M.R.E., Boicourt, R.M., 1975. NJOY: a neutron and photon processing system. Trans. Am. Nucl. Soc. 720.
- Farras Abdelnour, A., Selesnick, I.W., 2001. Design of 2-band orthogonal near-symmetric CQF. In: Proceedings of International Conference Acoustics, Speech, Signal Processing (ICASSP 2001), Salt Lake City, Utah, May2001, Institute of Electrical and Electronics Engineers.
- Giust, F.D., Stamm'ler, R.J.J., Ferri, A.A., 2001. HELIOS 1.7 User Guide and Manual. Studsvik Scandpower.
- Halsall, M.J., 1991. A review of the WIMS nuclear data library. Nucl. Energy 30, 285.

- Hébert, A., Marleau, G., 1991. Generalization of the Stamm'ler method for the self-shielding of resonant isotopes in arbitrary geometries. *Nucl. Sci. Eng.* 108, 230.
- Hébert, A., 2004. A mutual resonance shielding model consistent with ribbon subgroup equations. In: *Proceedings of International Meeting on the Physics of Fuel Cycles and Advanced Nuclear Systems PHYSOR 2004*.
- Hébert, A., 2007. A review of legacy and advanced self-shielding models for lattice calculations. *Nucl. Sci. Eng.* 155, 310–320.
- Knott, D., et al., 1995. *CASMO-4 Methodology Manual*. STUDSVIK/SOA-95/02, Studsvik of America.
- Le Tellier, R., Fournier, D., Ruggieri, J.M., 2009. A wavelet-based finite element method for the self-shielding issue in neutron transport. *Nucl. Sci. Eng.* 163, 34–55.
- Marleau, G., Hébert, A., Roy, R., 2000. *A User Guide for Dragon*. Ecole polytechnique de Montreal, Montreal.
- Newland, D.E., 1993. *An Introduction to Random Vibrations, Spectral and Wavelet Analysis*. John Wiley and Sons, New York.
- Nikolaev, M.N., Ignatov, A.A., Isaev, N.V., et al., 1970. The method of subgroups for considering the resonance structure of the cross section in neutron calculations. *Sov. Atom. Energy* 29, 689.
- NUREG/CR-0200, 1990. *SCALE: A Modular Code System for Performing Standardized Computer Analysis for Licensing Evaluation*, vols. I–IV. NUREG/CR-0200, Oak Ridge National Laboratory.
- O'Dell, R.D., Alcouffe, R.E., 1987. *Transport Calculations for Nuclear Analysis: Theory and Guidelines for Effective Use of Transport Codes*. LA-10983-MS, Los Alamos National Laboratory.
- Reuss, P., Coste-Delclaux, M., 2003. Development of computational models used in France for neutron resonance absorption in light water lattices. *Progress in Nuclear Energy* 42, 237–282.
- Sanchez, R., et al., 1990. Models for multigroup self-shielded cross section calculations in the code APOLLO2. In: *Proceedings of International Conference on Physics of Reactor Operation, Design, and Computation*, Marseille, France.
- Strang, G., 1989. Wavelets and dilation equations: a brief introduction. *SIAM Rev.* 31, 614.
- Tsuchihashi, K., Takano, H., Horikami, K., 1983. SRAC: JAERI thermal reactor standard code system for reactor design and analysis. JAERI 1285.
- Williams, M.L., Asgari, M., 1995. Computations of continuous-energy neutron spectra with discrete ordinates transport theory. *Nucl. Sci. Eng.* 121, 173.
- Worrall, A., 1999. Effect of plutonium vector on core wide nuclear design parameters. IAEA-SM-358/28.
- Zhong, Z., Thomas, J.D., Xu, Y., 2006. Continuous-energy multidimensional s_n transport for problem-dependent resonance self-shielding calculations. *Nucl. Sci. Eng.* 154, 190.
- Zheng, Y., Wu, H., Cao, L., 2009. An improved three-dimensional wavelet-based method for solving the first-order Boltzmann transport equation. *Ann. Nucl. Energy* 36, 1440–1449.